Post-Print

N.V. Muravyev, K.A. Monogarov, D. Prokopyev, A.A. Bragin, L. Galfetti, L.T. De Luca, A.N. Pivkina
Macro- vs Microcrystalline Wax: Interplay of Evaporation and Decomposition Under Pressure Variation
Energy & Fuels, Vol. 31, N. 8, 2017, p. 8534-8539
doi:10.1021/acs.energyfuels.7b00895

Macro- vs Microcrystalline Wax: Interplay of Evaporation and Decomposition under Pressure Variation

Nikita V. Muravyev[*†], Konstantin A. Monogarov[†], Dmitry Prokopyev[‡], Anatoly A. Bragin[†], Luciano Galfetti[‡], Luigi T. DeLuca[‡], Alla N. Pivkina[†]

† Semenov Institute of Chemical Physics, Russian Academy of Sciences, Moscow 119991, Russia

‡ Aerospace Science and Technology Department, Politecnico di Milano, Milan 20156, Italy

Abstract

Thermal behavior of two principally different wax materials (viz., paraffin Russian grade P-2 and microcrystalline Sasol 0907) has been investigated using thermogravimetry and differential scanning calorimetry at atmospheric and elevated pressure. The variation of experimental conditions during thermoanalytical studies highly affects the kinetics and highlights the interplay between evaporation and decomposition processes. It is revealed that vaporization kinetics is defined by the amount of the linear and branched hydrocarbons and under low confinement takes place with an enthalpy of $\Delta H_{ev}(298\ K) = 79 \pm 7$ kJ mol^{-1}. In turn, thermal decomposition with the activation energy equal to 236 ± 4 kJ mol^{-1} is shown to follow the random-scission reaction mechanism. The simultaneous consideration of obtained kinetic data reveals the general kinetic compensation trend and elucidates the unified underlying nature of the wax thermal response.

Introduction

Paraffin waxes find numerous applications including the hybrid rocket propulsion engines.(1-4) Recent activities showed that the paraffin-based fuels exhibit 3–4 times higher regression rates compared to hydroxyl-terminated polybutadiene (HTPB) compositions.(2) Two general types of petroleum waxes are produced, i.e., macrocrystalline wax (paraffin wax) and microcrystalline wax (derived from the residual distillate lubricating oil fraction).(5) Having a different content of the linear and branched hydrocarbons, the macro- and microcrystalline waxes reveal different functional properties (e.g., melting point, viscosity).(3)

The detailed understanding of the thermal response of the fuel is of paramount importance for applications in solid-fuel ramjet as well as for mathematical modeling of hybrid rocket engines.(1, 6) Despite its practical importance, the kinetics of thermally induced transformations in waxes is not fully understood. Hinshelwood et al. addressed the gas-phase paraffin decomposition kinetics in a series of papers.(7-9) However, the pyrolysis of wax involves its evaporation (10) and the

decomposition in liquid state. The interplay between these two processes is supposed to be dependent on pressure–temperature conditions.
Recently, we have shown (11) that high-pressure differential scanning calorimetry (HP-DSC) offers the benefit of the suppression of the evaporation thus allowing for the observation of the decomposition reaction. The present study explores the utilization of this experimental approach combined with the advanced thermokinetic modeling(12) and determination of the thermochemical parameters.(13) We have intended to obtain the kinetic representations of separated decomposition and evaporation processes for both types of waxes, having a different balance between linear and branched hydrocarbons, under various experimental conditions to generalize the findings.

Experimental Section

Materials

Microcrystalline wax Sasol 0907 (Sasol Performance Chemicals), denoted as CW, was investigated without any purification. As a paraffin wax the highly purified material of Russian grade P-2 (according to Standard GOST 23683-89) was used; this is designated as PW. High-temperature chromatographic analyses (Thermo Scientific instrument) for both waxes were performed up to 35 carbon numbers (Table S1, Supporting Information). FTIR spectra (Nicolet 5700, Thermo Electron) of both materials reveal the absence of aromatic hydrocarbons. Table 1 represents the literature data (3, 14, 15) supported by our findings. Paraffin wax contains mostly linear (n) alkanes, while the crystalline wax has about half of the branched (iso) hydrocarbons. The CW sample has a higher molecular mass compared to PW, consequently it is more viscous and has a higher melting point.

Table 1. Properties of Investigated Paraffin Wax Samples[a]

			content of alkanes/mass %		no. of carbon/min..max	
sample	trademark	melting point/°C	linear	branched	linear	branched
PW	P-2	51–53	87[14]	12[14]	19..36[14]	23..39[14]
CW	Sasol 0907	50–110	36[15]	64[15]	22..64[3]	28..86[3]

[a] In ref 3 data corresponds to the fractions with content >10 wt %.

Thermoanalytical Methods

Thermal behavior was studied with a DSC 204 HP (Netzsch) apparatus at environmental pressures of 0.1, 1, and 5 MPa. Samples of 5.05 ± 0.05 mg mass were used; for Sasol 0907 this corresponds to 1/4 part of one prill. Paraffin wax was placed in closed Al pans with an internal diameter of 5.5 mm and laser-cut pinholes ca. 300 μm, i.e., semiclosed conditions. To cover a broad range of temperatures we perform the nonisothermal runs with constant heating rates of 5, 10, 20, and 40 K min^{-1} under nitrogen flow 100 mL min^{-1}. All calibrations were performed according to manufacturer recommendations by conducting experiments on melting of pure (>99.999%) In, Bi, Zn, and Sn metals under the same conditions as used for kinetic data acquisition.
Thermogravimetric signals (TGA) were recorded with an STA 449 F3 (Netzsch) thermal analyzer. Samples of 5.0 ± 0.1 mg mass were placed in open alumina pans and heated with rates of 1, 2, 5, and 10 K min^{-1} under argon flow of 70 mL min^{-1}. Thermogravimetric data were used to reveal the evaporation enthalpy. Under certain conditions (low confinement, low heating rates, etc.) the Langmuir equation can be used to derive the vaporization enthalpy $\Delta H_{ev}(T)$ at the average experimental temperature $\overline{T}$(16)

$$\ln\left(\frac{dm}{dt}\sqrt{T}\right) = a - \frac{\Delta H_{ev}(\overline{T})}{RT} \qquad (1)$$

where d*m*/d*t* stands for the mass loss rate, and *a* is a constant. Thus, the obtained vaporization enthalpy was converted to the standard value at 298 K using Sidgwick's rule proven to be reliable over a wide range of hydrocarbons:(17)

$$\Delta H_{ev}(298\ \mathrm{K}) = \Delta H_{ev}(\overline{T}) + 0.054(\overline{T} - 298) \quad (2)$$

The implemented method of the vaporization enthalpy determination has been verified over a range of the reference hydrocarbon and energetic species.(13) Additionally, at 10 K min^{-1} FTIR spectra of the gases evolved were registered simultaneously with DSC and TGA data. A novel type of IR spectrometer connection was used to provide the minimal path for gas flow.(18)

Kinetic Techniques

For kinetic analysis, the self-developed THINKS(19) software package was used. The code comprises the main modern thermokinetic methods and has been successfully applied to some complex reactions.(12, 20) At first, the isoconversional Friedman method(21) was applied showing the variation of the effective kinetic parameters *A* and E_a with the conversion degree α

$$\ln\left(\frac{\mathrm{d}\alpha}{\mathrm{d}t}\right)_{\alpha,i} = \ln[f(\alpha)A_\alpha] - \frac{E_\alpha}{RT_{\alpha,i}} \quad (3)$$

where *i* refers to a particular measurement. Then, if the process seems to be governed by a single-step, the combined kinetic analysis(22) was used to determine the resulting kinetic parameters. For the data that established two or more reaction steps, the formal kinetic approach was applied. Thus, thermoanalytical DSC data were fitted with a consecutive, parallel, or independent combination of various ideal reaction models.(23) In most cases, the best fit was obtained with the reaction model in the form of the so-called reduced Sestak–Berggren equation(24)$f(\alpha) = c\alpha^m(1-\alpha)^n$(4)where the reaction order *n* and the exponent *m* are adjusted parameters, in some combinations leading to the ideal reaction types.(22) To decrease the correlation between pre-exponential factor *A* and activation energy E_a during the nonlinear regression, a method based on scaling of the parameters and its reparametrization with local (mean) temperature was used.(25)

Results and Discussion

Thermal Behavior at 0.1 MPa

Once heated from the room temperature, both wax samples reveal first the broad endothermic melting peaks (Figure 1). The position of melting endotherms agrees with the amount of hydrocarbon fractions – alkanes with higher carbon numbers in the CW sample result in higher melting point, while its broader distribution on molecular mass reflects the wider temperature range of the phase transition compared to PW. The second thermal effect on DSC curves at 400–500 °C is attributed to the degradation of wax. Apparently, during this step the evaporation and decomposition processes are superimposed.

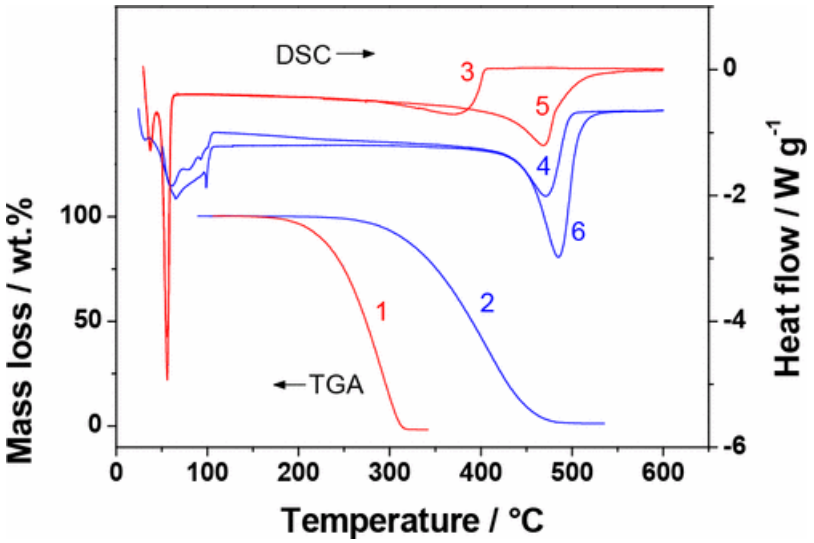

Figure 1. TGA (curves 1, 2) and DSC data obtained at 0.1 (curves 3, 4) and 1 MPa (curves 5, 6): PW (curves 1, 3, 5) and CW (curves 2, 4, 6) samples, heating rate of 10 K min^{-1}. DSC traces are shifted for clarity.

Further exploring of the process at atmospheric pressure was conducted using thermogravimetry, while the wax samples were heated in open pans under argon flow. FTIR spectra of evolved gas-phase products were registered in situ. Compared to DSC data, samples were unconfined and one can expect its easier evaporation. The relative position of the mass-loss curves conforms the molecular mass difference – the lighter PW evaporates before the CW sample (Figure 1). Analysis of FTIR spectra for both wax samples reveals that the combination of the vibration frequencies is the same for the evolved gases and the starting solid (Figure 2, Figure S2, Supporting Information). As-received materials represent mixtures of hydrocarbons and so apparently does the registered gas-phase. Differences in the relative intensity for the signals of gas phase as compared to the solid could arise from the changes in composition due to the decomposition or from different experimental conditions (devices, procedures, etc.). Moreover, some kind of decomposition can occur not in the thermal analyzer but during the gas transition to the FTIR spectrometer or inside it.

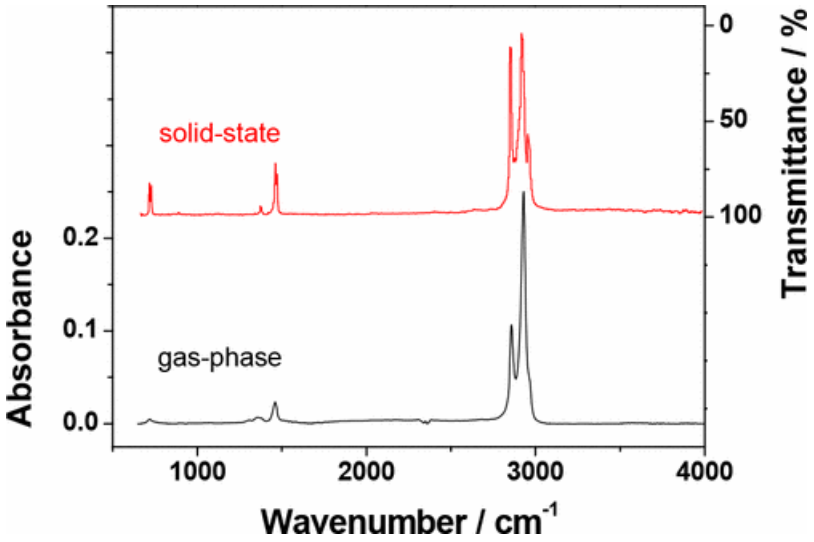

Figure 2. FTIR spectra obtained on solid PW (red curve) and evolved gases during PW heating to 350 °C (black).

Isoconversional analysis of TGA data for PW, which is composed mostly of linear alkanes, reveals a relatively constant activation energy through the conversion (Figure 3). The resulting value of ca. 70

kJ mol^{-1} is in the range typical for the vaporization, which supposed to occur. Thus, the evaporation enthalpy was extracted using eqs 1 and 2 and the experimental TGA data. For macrocrystalline wax, the resulting value of ΔH_{ev} corrected to 298 K is 79 ± 7 kJ mol^{-1} (see Table S2, Supporting Information for details). This result agrees with heat of vaporization equal to 71 kJ mol^{-1} (163.5 J g^{-1}) reported by Karabeyoglu et al.(1) for a paraffin wax with an average formula $C_{31}H_{64}$.

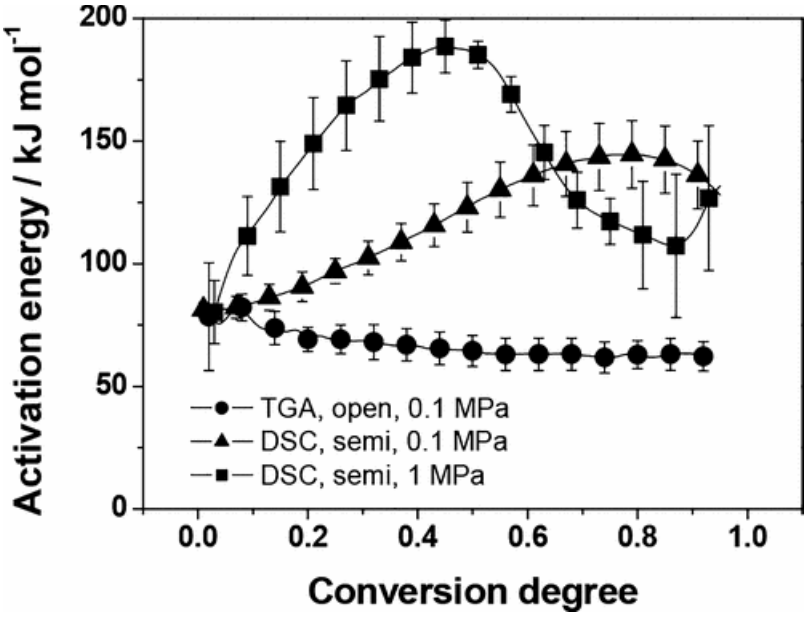

Figure 3. Isoconversional plot for paraffin wax (PW).

A formal kinetic description of thermogravimetric data (Figure S3a, Supporting Information) shows that the process consists of two independent stages, which explain the variation in isoconversional results. The optimized kinetic parameters for these stages are presented in Table 2. The first step with the contribution to the total mass loss, η = 0.90 ± 0.05, apparently corresponds to the linear alkanes evaporation, while the second step corresponds to a process for the branched hydrocarbons. Due to the very low contribution of the second process, the uncertainties in its kinetic parameters are relatively high. Nevertheless, the conclusion about its larger activation energy can be drawn.

Table 2. Kinetic Parameters for Fitting with Single Reactions Eq 4 or Its Combination for Wax Samples

sample	conditions	Q/J g^{-1}	lg$A$/s^{-1}	E_a/kJ mol^{-1}	reaction order n	exponent m
CW	TGA, 0.1 MPa	–	8 ± 3	129 ± 3	1.1 ± 0.2	–0.9 ± 0.1
		–	15 ± 4	235 ± 34	1.7 ± 0.3	0[a]
	DSC, 0.1 MPa	–250 ± 10	15.5 ± 0.2	250.4 ± 0.9	0.90 ± 0.01	0.18 ± 0.01
	DSC, 1 MPa	–500 ± 15	14.4 ± 0.3	236 ± 4	1.06 ± 0.04	0.35 ± 0.04
PW	TGA, 0.1 MPa	–	3.8 ± 1.0	68.8 ± 1.5	0.13 ± 0.08	0[a]
		–	10 ± 5	120 ± 16	0[a]	0[a]
	DSC, 0.1 MPa	–220 ± 10	6.7 ± 0.7	114 ± 2	0.19 ± 0.09	0[a]
			3.2 ± 0.5	69 ± 1	0[a]	0[a]
	DSC, 1 MPa	–290 ± 20	3.9 ± 0.3	85 ± 5	0.89 ± 0.11	0.36 ± 0.04
			13.6 ± 1.9	216 ± 14	1.75 ± 0.17	0.57 ± 0.06

[a] Value fixed in calculations.

Isoconversional data for microcrystalline wax reveals the plateau ca. 120 kJ mol^{-1} at low conversion followed by the rise to ca. 250 kJ mol^{-1} at the final stage (Figure 4). Formal kinetic analysis reveals

the best to be a model with two independent stages (η = 0.80 ± 0.04). The activation energy values for stages (Table 2) agree with the isoconversional observations. Nondigit reaction order *n* and exponent *m* values are the apparent parameters affected by the complexity of the material itself being a mixture of various hydrocarbons and the reaction conditions. To distinguish the kinetic information on constituting steps of the overall pyrolysis, the reaction conditions were probed, i.e., the elevated pressure applied, and the thermokinetic analysis on the experimental data thus obtained performed.

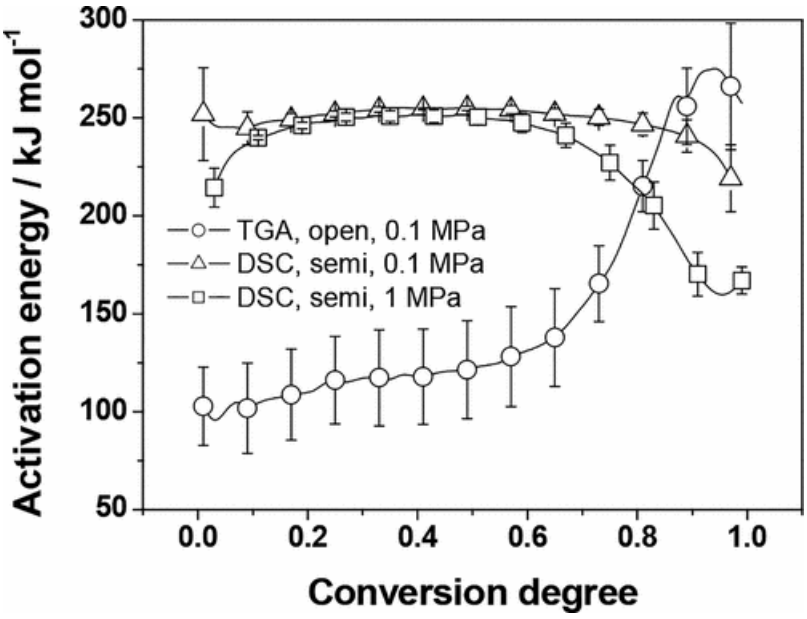

Figure 4. Isoconversional plot for microcrystalline wax (CW).

Pyrolysis of Microcrystalline Wax (CW) at Elevated Pressures

Figure 1 illustrates that at higher pressure the higher endothermic heat effect is observed, while the temperature range of transformation remains unaffected. For the dominant reaction near the minimum of the DSC signal, a rough estimate of the kinetic parameters can be obtained with the Kissinger method.(26) Thus, the apparent activation energy values are 266 ± 7, 263 ± 6, and 280 ± 30 kJmol^{-1}, and preexponential factor values are 16.6 ± 0.5, 16.1 ± 0.4, and 17 ± 2 s^{-1} at pressures of 0.1, 1, and 5 MPa correspondingly. Considering the inaccuracies in the parameters, these values appear to be independent of pressure. The isoconversional results agree with this conclusion – the coinciding stage around 250 kJ mol^{-1} is evident in Figure 4. The refinement of the kinetic parameters has been achieved with the formal kinetic analysis; the results are listed in Table 2. Further insight into the process can be obtained from the effective exponents *n*, *m* by the analysis of the reaction model function using reduced master plots.(27) Figure 5 illustrates the pressure influence, which results in a single-step overall kinetics and brings the reaction model to the L2-type dependency. The kinetic equation of this type has been proposed by Flynn and Wall(28) based on the theoretical model of Simha and Wall(29) for the description of the degradation of polymers driven by random scission. Assuming that the process follows the first order law

$$\frac{dx}{dt} = k(1 - x)$$

the total conversion degree α can be expressed by

$$1 - \alpha = (1 - x)^{L-1}\left[1 + x\frac{(N - L)(L - 1)}{N}\right]$$

where x is the fraction of the broken bonds, N is the initial degree of polymerization, and L is the number of groups (e.g., ═CH_2) in the smallest chain, which does not evaporate before being further degraded. Usually $N \gg L$ and the equation can be simplified. However, the symbolic solution is possible only for $L = 2$, leading to L2-mode,(30) which we obtain experimentally.

$$f(\alpha) = 2(\alpha^{1/2} - \alpha)$$

Thus, at elevated pressure, when the evaporation is effectively suppressed, the dominant process of the pyrolysis becomes the single random-scission reaction.

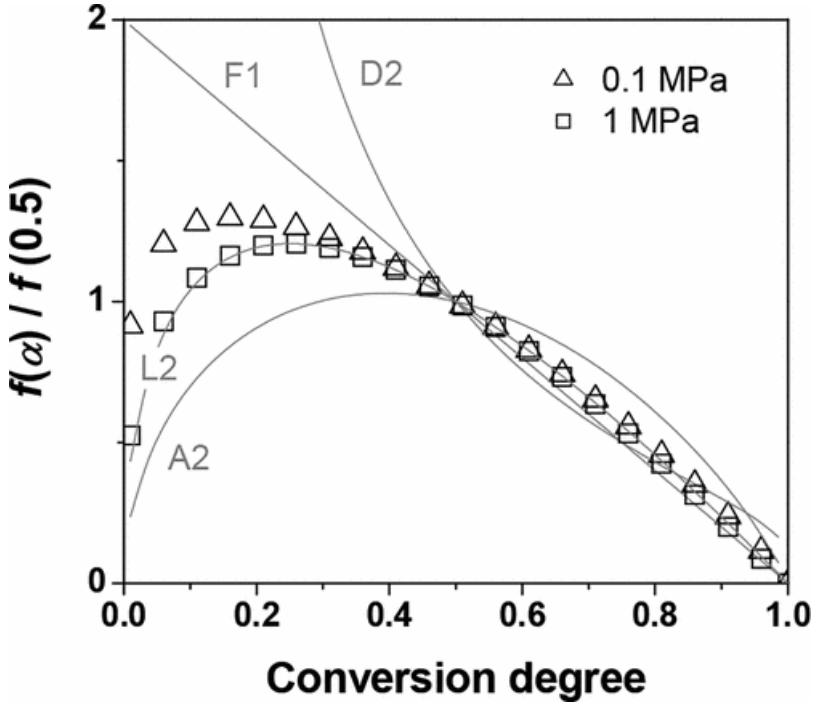

Figure 5. Master plot illustrating the results for CW pyrolysis under 0.1 and 1 MPa compared with the literature proposed ideal reaction types. Several kinetic models are shown including first-order reaction (F1), two-dimensional diffusion (D2), random scission (L2), and Avrami-Erofeev reaction (A2).

Pyrolysis of Macrocrystalline Wax (PW) at Elevated Pressures

Starting from the TGA in open pans we increase first the confinement (DSC, semiclosed pans, 0.1 MPa) and then the pressure (DSC, semiclosed pans, 1 MPa), observing the higher complexity of thermal transformations (Figure 1, Figure S5, Supporting Information). For the DSC experiments at 0.1 MPa the isoconversional analysis reveals that the activation energy at the beginning is equal to the evaporation enthalpy determined above and then rises to ca. 130 kJ mol^{-1}. The best formal kinetic model is obtained with two independent steps ($\eta = 0.75 \pm 0.07$) having almost zero exponents n, m indicating the apparent nature of evaporation.

The isoconversional activation energy for measurements at 1 MPa pressure starts from the same value as for 0.1 MPa corresponding to the evaporation enthalpy, then increases up to 200 kJ mol^{-1}, and finally stabilizes at ca. 120 kJ mol^{-1} (Figure 3). As in previous case, the introduction of two independent stages is enough to reveal a good fit of the experimental data. Whereas the first reaction has both kinetic parameters low and characteristic of the vaporization process, the second stage

parameters are close to the reaction observed above for the microcrystalline wax at elevated pressures, i.e., the liquid-state decomposition.

General Model of Thermal Behavior

The kinetic parameters for two different wax types under various experimental conditions are summarized in Table 2. Are these microcrystalline and paraffin waxes different in terms of thermal behavior? Figure 6 graphically represents the kinetic information obtained so far. First, one can notice that all kinetic pairs lie around the consistent lg$A$(E_a) line, i.e., exhibit the so-called kinetic compensation effect (KCE). The kinetic compensation effect, although widely discussed in the past literature, (31, 32) even now is a subject of debates.(33) There are several proposed origins of the "false" KCE including the experimental errors,(34) inappropriate mathematical treatment (e.g., with incorrect model (35)), impact of the reversible reactions,(36) or partial pressure of a gaseous products.(37) Contrary, the "true" kinetic compensation can be an indication of the common physicochemical nature behind the data. Results of the present study, obtained for two substances under different experimental conditions, apparently represent the KCE reflected by the unique nature of the wax pyrolysis.

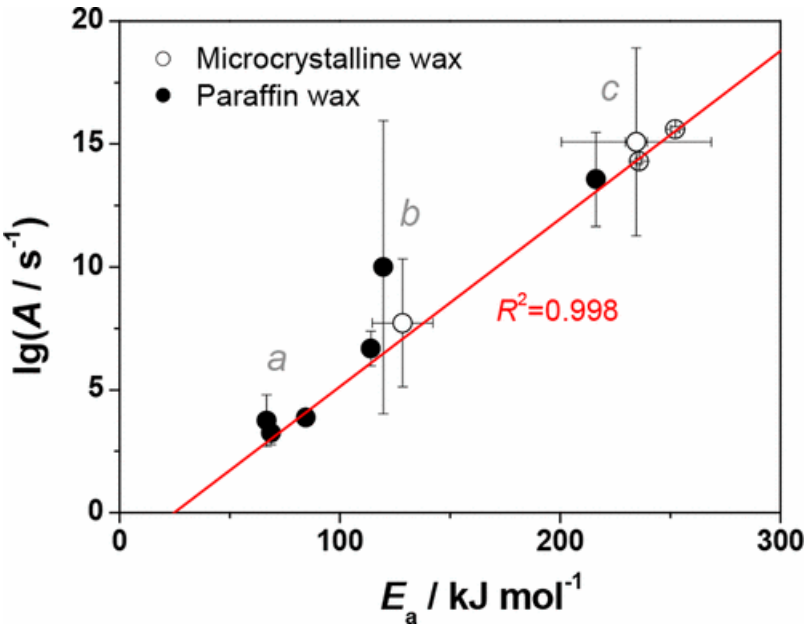

Figure 6. Kinetic compensation of the obtained kinetic parameters. Points are the values from Table 2.

Careful observation of Figure 6 suggests the existence of three intervals of the activation energy values, i.e., around 70, 120, and 230 kJ mol^{-1}. Analysis of these kinetic parameters allows the proposal of the general descriptive model of the process, which is schematically presented in Figure 7. Both studied materials contain two main components, i.e., linear and branched hydrocarbons. Being heated, hydrocarbons evaporate when low confinement is applied leading to the two corresponding mass loss steps, as it is observed for paraffin wax. For linear alkanes, due to its majority in paraffin wax, the evaporation enthalpy was determined to be ΔH_{ev}(298 K) = 79 ± 7 kJ mol^{-1} in agreement with the literature value.(1) Note that the evaporation enthalpy at an average measurement temperature (i.e., the apparent activation energy) is less by 10 kJ mol^{-1} according to eq 2. The evaporation of the branched hydrocarbons is significant for CW pyrolysis in open pans and for PW at elevated pressure (rows #1, 6, and 7 in Table 2) with the suggested value of 114 ± 2 kJ mol^{-1}. These two evaporation steps are denoted as "a" and "b" in Figure 7.

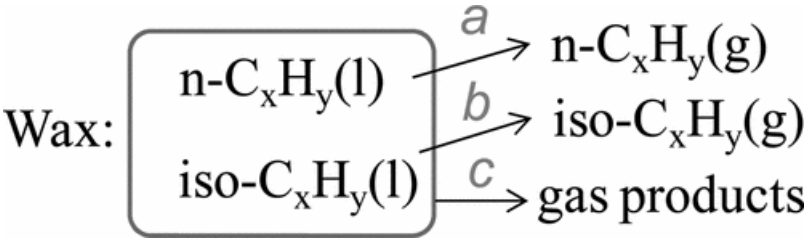

Figure 7. Generalized scheme of the wax pyrolysis.

When confinement of the system becomes significant, the activation energy rises to 236 ± 4 kJmol^{-1}, and the reaction model follows the random-scission reaction mechanism. This step, marked as "c" in Figure 7, is observed for both microcrystalline and paraffin waxes (rows #2, 3, 4, and 10 in Table 2). It is interesting to compare the results with the reported values for the paraffin decomposition. (7-9, 38) Two main reactions were considered in the literature, viz. the molecular rearrangement and the chain reaction. With ascent of the hydrocarbon series and with increasing pressure of paraffin vapor (10^{-5}–0.2 MPa), the role of the molecular rearrangement process is shown to become more important. The reaction order is reported to vary between the first and the second (9) or lie in the range 1–1.17 (38) in accordance with roughly first order obtained in the present work. At high pressures of the hydrocarbon vapor, the obtained activation energy values are in the range of 235–265 kJ mol^{-18} agreeing well with our proposal for stage "c".

Thus, the overall pyrolysis process of both microcrystalline and paraffin waxes is governed by competitive evaporation and decomposition. The specific composition of the wax, i.e., the ratio of the linear and branched hydrocarbons and its distribution on the carbon numbers, defines the vaporization kinetics. Along with the wax properties, the experimental conditions of thermoanalytical measurements, i.e., the degree of confinement and the applied pressure, also influence on the relative contribution of the evaporation and decomposition stages. We propose a comprehensive approach to vary all the above factors with the subsequent kinetic parameters analysis for deriving the unified underlying kinetic features.

Conclusions

Microcrystalline and macrocrystalline waxes represent the complex objects consisting of two principal components with a broad distribution of hydrocarbons over the carbon numbers. Varying the operating conditions of the thermoanalytical experiments and comparing the two wax samples, the general descriptive scheme of their pyrolysis was suggested. Depending on the operating conditions, the evaporation of the constituting hydrocarbons, decomposition in vapor, or its combinations were observed. The overall kinetic scheme contains three main stages, i.e., the evaporation of the linear alkanes, the evaporation of the branched hydrocarbons, and thermal decomposition. The first process was analyzed in the frame of the Langmuir model, and its evaporation enthalpy was determined to be ΔH_{ev}(298 K) = 79 ± 7 kJ mol^{-1}. The second stage was not purely distinguished; however, the value of 114 ± 2 kJ mol^{-1} is recommended for the evaporation of the branched hydrocarbons fraction from macro- and microcrystalline waxes. Thermal decomposition becomes dominant at elevated environmental pressure leading to the process with the barrier of 236 ± 4 kJ mol^{-1} driven by the random-scission mechanism. The results are believed to help in predicting the thermal response during manufacturing and can be incorporated in the modern models for the hybrid rocket propulsion engines.

Acknowledgment

N.V.M., K.A.M., A.A.B., and A.N.P. acknowledge the Russian Foundation for Basic Research for financial support (project 16-29-01055 ofi_m).

References

1. Karabeyoglu, M. A.; Altman, D.; Cantwell, B. J. J. Propul. Power 2002, 18 (3) 610– 620 DOI: 10.2514/2.5975
2. Fundamentals of Hybrid Rocket Combustion and Propulsion; Kuo, K. K.; Chiaverini, M. J., Eds.; American Institute of Aeronautics and Astronautics: Reston, VA, 2007; DOI: DOI: 10.2514/4.866876 .
3. Piscitelli, F.; Saccone, G.; Gianvito, A.; Cosentino, G.; Mazzola, L. In Proceedings of the 6th European conference for aeronautics and space sciences (EUCASS); 2015; pp 1– 13.
4. Kobald, M.; Schmierer, C.; Ciezki, H. K.; Schlechtriem, S.; Toson, E.; De Luca, L. T. J. Propul. Power 2017, 1– 7 DOI: 10.2514/1.B36207
5. Fuels and lubricants handbook: technology, properties, performance, and testing; Totten, G. E.; Westbrook, S. R.; Shah, R. J., Eds.; ASTM manual series; ASTM International: West Conshohocken, PA, 2003.
6. Karabeyoglu, A.; Cantwell, B.; Stevens, J. In Proceedings of 41st AIAA/ASME/SAE/ASEE Joint Propulsion Conference & Exhibit; 2005, pp. 1− 42. DOI: 10.2514/6.2005-3908 .
7. Stubbs, F. J.; Hinshelwood, C. Proc. R. Soc. London, Ser. A 1950, 200 (1063) 458– 473 DOI: 10.1098/rspa.1950.0031
8. Ingold, K. U.; Stubbs, F. J.; Hinshelwood, C. Proc. R. Soc. London, Ser. A 1950, 203 (1075) 486– 501 DOI: 10.1098/rspa.1950.0152
9. Stubbs, F. J.; Ingold, K. U.; Spall, B. C.; Danby, C. J.; Hinshelwood, C. Proc. R. Soc. London, Ser. A 1952, 214 (1116) 20– 35 DOI: 10.1098/rspa.1952.0147
10. Boiocchi, M.; Milova, P.; Galfetti, L.; Di Landro, L.; Golovko, A. K. In Progress in Propulsion Physics, EUCASS Proceedings Series; 2016, 8, 241– 262. DOI: 10.1051/eucass/201608241 .
11. Muravyev, N. V.; Monogarov, K. A.; Bragin, A. A.; Fomenkov, I. V.; Pivkina, A. N. Thermochim. Acta 2016, 631, 1– 7 DOI: 10.1016/j.tca.2016.03.018
12. Muravyev, N. V.; Koga, N.; Meerov, D. B.; Pivkina, A. N. Phys. Chem. Chem. Phys. 2017, 19 (4) 3254– 3264 DOI: 10.1039/C6CP08218A
13. Muravyev, N. V.; Pivkina, A. N.; Kiselev, V. G. J. Chem. Eng. Data 2017, 62 (1) 575– 576 DOI: 10.1021/acs.jced.6b00483
14. Lysenko, S. V.; Kulikov, A. B.; Onishchenko, M. I.; Maksimov, A. L.; Rakhmanov, E. V.; Karakhanov, E. A. Moscow Univ. Chem. Bull. 2016, 71 (1) 37– 44 DOI: 10.3103/S0027131416010090
15. Grosse, M. In Proceedings of 45th AIAA/ASME/SAE/ASEE Joint Propulsion Conference & Exhibit; 2009, pp. 1− 25. DOI: 10.2514/6.2009-5113 .
16. Price, D. M. Thermochim. Acta 2015, 622, 44– 50 DOI: 10.1016/j.tca.2015.04.030
17. Sidgwick, N. V. Some Physical Properties of The Covalent Link in Chemistry; Cornell University Press: London, 1933.
18. Schindler, A.; Neumann, G.; Rager, A.; Füglein, E.; Blumm, J.; Denner, T. J. Therm. Anal. Calorim. 2013, 113 (3) 1091– 1102 DOI: 10.1007/s10973-013-3072-9
19. Muravyev, N. V.THINKS – thermokinetic software; Moscow, 2016.
20. Muravyev, N. V.; Monogarov, K. A.; Asachenko, A. F.; Nechaev, M. S.; Ananyev, I. V.; Fomenkov, I. V.; Kiselev, V. G.; Pivkina, A. N. Phys. Chem. Chem. Phys. 2017, 19, 436– 449 DOI: 10.1039/C6CP06498A
21. Friedman, H. L. J. Polym. Sci., Part C: Polym. Symp. 1964, 6 (1) 183– 195 DOI: 10.1002/polc.5070060121

22. Pérez-Maqueda, L. A.; Criado, J. M.; Sánchez-Jiménez, P. E. J. Phys. Chem. A 2006, 110 (45) 12456– 12462 DOI: 10.1021/jp064792g
23. Vyazovkin, S.; Burnham, A. K.; Criado, J. M.; Pérez-Maqueda, L. A.; Popescu, C.; Sbirrazzuoli, N. Thermochim. Acta 2011, 520 (1–2) 1– 19 DOI: 10.1016/j.tca.2011.03.034
24. Burnham, A. K. J. Therm. Anal. Calorim. 2000, 60 (3) 895– 908 DOI: 10.1023/A:1010163809501
25. Pomerantsev, A. L.; Kutsenova, A. V.; Rodionova, O. Y. Phys. Chem. Chem. Phys. 2017, 19 (5) 3606– 3615 DOI: 10.1039/C6CP07529K
26. Kissinger, H. E. Anal. Chem. 1957, 29 (11) 1702– 1706 DOI: 10.1021/ac60131a045
27. Criado, J. M.; Pérez-Maqueda, L. A.; Gotor, F. J.; Málek, J.; Koga, N. J. Therm. Anal. Calorim. 2003, 72 (3) 901– 906 DOI: 10.1023/A:1025078501323
28. Flynn, J. H.; Wall, L. A. J. Res. Natl. Bur. Stand., Sect. A 1966, 70A (6) 487 DOI: 10.6028/jres.070A.043
29. Simha, R.; Wall, L. A. J. Phys. Chem. 1952, 56 (6) 707– 715 DOI: 10.1021/j150498a012
30. Sánchez-Jiménez, P. E.; Pérez-Maqueda, L. A.; Perejón, A.; Criado, J. M. Polym. Degrad. Stab. 2010, 95 (5) 733– 739 DOI: 10.1016/j.polymdegradstab.2010.02.017
31. Garn, P. D. J. Therm. Anal. 1975, 7 (2) 475– 478 DOI: 10.1007/BF01911956
32. Agrawal, R. K. J. Therm. Anal. 1986, 31 (1) 73– 86 DOI: 10.1007/BF01913888
33. Barrie, P. J. Phys. Chem. Chem. Phys. 2012, 14 (22) 8235 DOI: 10.1039/c2cp41022b
34. Barrie, P. J. Phys. Chem. Chem. Phys. 2012, 14 (1) 318– 326 DOI: 10.1039/C1CP22666E
35. Vyazovkin, S. V.; Lesnikovich, A. I. Thermochim. Acta 1990, 165 (1) 11– 15 DOI: 10.1016/0040-6031(90)80201-9
36. Galwey, A. K.; Brown, M. E. Thermochim. Acta 1997, 300 (1–2) 107– 115 DOI: 10.1016/S0040-6031(96)03120-6
37. Ray, H. S. J. Therm. Anal. 1982, 24 (1) 35– 41 DOI: 10.1007/BF01914797
38. Partington, R. G.; Stubbs, F. J.; Hinshelwood, C. N. J. Chem. Soc. 1949, 2674 DOI: 10.1039/jr9490002674